Structure-property relationship of pH-sensitive (PCL) 2 (PDEA- b -PPEGMA) 2 micelles: Experiment and DPD simulation

ARTICLE *in* AICHE JOURNAL · OCTOBER 2014

Impact Factor: 2.75 · DOI: 10.1002/aic.14562

6 AUTHORS, INCLUDING:

Wenjing Lin
South China University of Technology
7 PUBLICATIONS **29** CITATIONS
SEE PROFILE

Yu Qian
South China University of Technology
203 PUBLICATIONS **1,604** CITATIONS
SEE PROFILE

Structure–Property Relationship of pH-Sensitive $(PCL)_2$ $(PDEA\text{-}b\text{-}PPEGMA)_2$ Micelles: Experiment and DPD Simulation

Wen Jing Lin, Shu Yu Nie, Quan Chen, Yu Qian, Xiu Fang Wen, and Li Juan Zhang
School of Chemistry and Chemical Engineering, South China University of Technology, Guangzhou 510640 P. R. China

DOI 10.1002/aic.14562
Published online August 1, 2014 in Wiley Online Library (wileyonlinelibrary.com)

The experiment and dissipative particle dynamics simulation were carried out on four polymers with different block ratios for the investigation of the structure–property relationship of (poly(ε-caprolactone)$_2$-[poly(2-(diethylamino)ethyl methacrylate)-b-*poly(poly(ethylene glycol) methyl ether methacrylate)]$_2$ [(PCL)$_2$(PDEA-b-PPEGMA)$_2$] micelles. The miktoarm star polymers assembled into spherical micelles composed of PCL core, pH-sensitive PDEA mesosphere and poly (ethylene glycol) methyl ether methacrylate (PPEGMA) shell. When decreasing pH from 7.4 to 5.0, the hydrodynamic diameter and transmittance of (PCL)$_2$(PDEA-b-PPEGMA)$_2$ micelles increased along with globule-uneven-extended conformational transitions, owing to the protonation of tertiary amine groups of DEA at lower pH conditions. Doxorubicin (DOX) was mainly loaded in the pH-sensitive layer, and more DOX were loaded in the core when increasing drug concentrations. The in vitro DOX release from the micelles was significantly accelerated by decreasing pH from 7.4 to 5.0. The results demonstrated that the pH-sensitive micelles could be used as an efficient carrier for hydrophobic anticancer drugs, achieving controlled and sustained drug release.* © 2014 American Institute of Chemical Engineers *AIChE J*, 60: 3634–3646, 2014

Keywords: multiscale, self-assembly, micelles, controlled drug delivery, release, pH-sensitivity

Introduction

An ever-increasing types of stimuli (pH, temperature, redox, light, ultrasound, and enzyme) are being explored on the environmental sensitive micelles in recent years.[1–4] Especially, the pH-sensitive micelles currently have attracted much attention as smart drug delivery systems for cancer therapy. An ideal anticancer pH-sensitive micelle can remain stable in normal tissues (pH 7.4) while release drugs rapidly in tumoral conditions (pH 5.0).[5–8] Although pH-sensitive micelles have been extensively investigated, it is still highly demanded to make a deeper understanding of structural transformation and drug release mechanism at varying pH conditions.

Star-shaped polymers, having similar topological structures to polymeric micelles and can form more stable nanoscale assemblies in selective solvents, have been actively investigated currently for potential utility as nanoreactors, catalysts, sensors, polymer electrolytes, and in biomedical and therapeutic applications.[9–13] Amphiphilic miktoarm star polymers (A_mB_n) with at least two different polymer chains emanating from the central core such as A_2B_2, A_3B_3, A_2B, A_3B, ABC, AB_2C_2, and ABCD, have been used in self-assembly and responsive behavior. Shen's group have synthesized a series of A_2B_2 miktoarm star copolymer C4S$(PCL)_2$-$(PEG)_2$, which could self-assemble into various morphologies in aqueous solution controlled by both the macromolecular architecture and composition of the copolymer.[14] Well-defined $(PNIPAAM)_2(PNVP\text{-}b\text{-}PAA)_2$ and $(PNIPAAM\text{-}b\text{-}PAA)_2(PNVP)_2$ have been developed by Zhu's group, and by tuning pH values and temperatures of aqueous solution of these two copolymers, three types of micellar aggregates and the unimer state could undergo reversible switch on and off in size and morphology.[15] However, limited work of A_2B_2- and A_3B_3-type miktoarm polymers was reported on the pH-sensitive drug release behavior.

Up to now, a range of experimental techniques have been used to investigate the dynamical and structural properties of polymeric micelles system, such as fluorescence probe technique, UV-VIS spectroscopy, dynamic light scattering (DLS), scanning electron microscopy, and transmission electron microscopy (TEM). However, the detailed information on the self-assembled behavior of the polymers from the experiment is difficult to obtain, because the micelles formed by polymer molecules are at nanometer scale. The structures and dynamics are hard to investigate deeply and directly by the present experiment methods. Aiming to address the limitation of the experiments, computer simulations have become a powerful analytical approach for enhancing the understanding of the experimental systems, which provide additional information on dynamics, distributions, and ordering of the morphologies.[16–21] Among usual computer simulation methods, for instance MD simulation whose time scales are

Additional Online Information may be found in the online version of this article.

Wen Jing Lin and Shu Yu Nie contributed equally to this work.

Correspondence concerning this article should be addressed to L. J. Zhang at celjzh@scut.edu.cn.

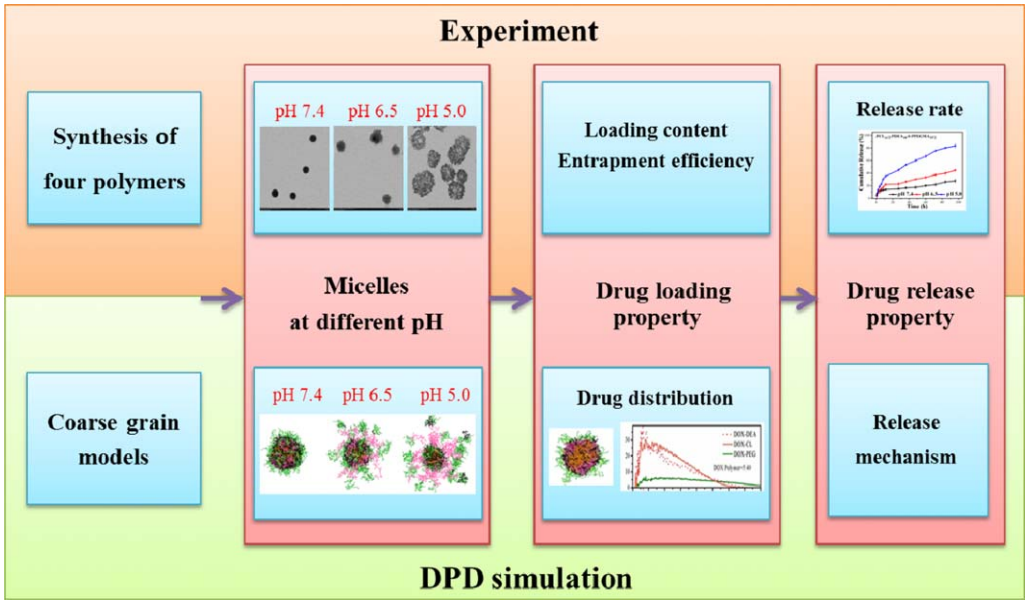

Scheme 1. Experiment and DPD simulation to study the structure and property of miktoarm star polymers.

[Color figure can be viewed in the online issue, which is available at wileyonlinelibrary.com.]

too short to observe the formation of the micelles, and the simulation at atom level is also very expensive, dissipative particle dynamics (DPD) which allows for a much larger time step and length scales is commonly used in the simulation of the fluids systems. Although less detailed than MD, DPD still enables a systematic study on the structural property of micelles and pH-sensitive drug release mechanism depended on the components of the polymers.[22–25]

In our recent work, DPD simulation study was carried out on the formation of DOX-loaded polymeric micelles formed by pH-sensitive amphiphilic homo-arm star polymer in neutral environment, effect of DOX content on morphologies of micelles, effect of pH value on morphologies of blank and DOX-loaded micelles, and so forth, which was without sufficient experimental results as a background.[26] Herein, the pH-sensitive amphiphilic $A_2(BC)_2$ miktoarm star polymers $(PCL)_2(PDEA\text{-}b\text{-}PPEGMA)_2$ with different block ratios were synthesized and used as an integrated platform for intracellular delivery of the anticancer drug DOX. Their self-assembled spherical micelles were composed of PCL core, pH-sensitive PDEA mesosphere, and poly (ethylene glycol) methyl ether methacrylate (PPEGMA) shell. In solutions, with different pH values, PDEA present different forms because of the protonation of amino groups. The PDEA layer is hydrophobic and collapses on the core at the physiological pH to prevent the premature burst drug release, but it becomes highly positively charged by protonation after being endocytosed by tumor cells, leading to faster release of the entrapped drug into the cytosol. The effect of pH values on the microstructures of the self-assembled drug-loaded micelles was simulated using DPD method. Furthermore, in this work, DPD simulations were performed based on real experimental systems for detailed information on the microstructures, drug distributions, and pH-release properties of the micelles formed by $(PCL)_2(PDEA\text{-}b\text{-}PPEGMA)_2$ with different block ratios. The scheme of experiment and DPD simulation was shown in Scheme 1. By combining experimental systems with DPD simulations, the structure–property relationship of the pH-responsive micelles were studied, which is beneficial to the optimal design of our polymers according to the expected drug delivery property.

Experimental Section

Materials

Pentaerythritol was dried under reduced pressure overnight prior to use. ε-Caprolactone (ε-CL, 99%, Aldrich) was dried over calcium hydride and distilled under reduced pressure before use. 2-(Diethylamino) ethyl methacrylate (DEA, TCI-EP) was distilled from calcium hydride, and stored under argon at −20°C. PEGMA ($M_n = 475$ Da, 99%, Aldrich) was purified by passing through a column filled with neutral alumina to remove inhibitor. Tetrahydrofuran (THF) was dried over sodium using benzophenone as a dryness indicator and distilled under nitrogen prior to use. Toluene was distilled from calcium hydride. Doxorubicin hydrochloride (DOX·HCl) was purchased from Beijing Huafeng United Technology CO., Pyrene (99%, Aldrich), 2-bromoisobutyryl bromide (98%, Alfa Aesar), 1,1,4,7,10,10-hexamethyltriethylenetetramine (HMTETA, 99%, Aldrich), $CuBr_2$, methanol, stannous octoate ($Sn(Oct)_2$), triethylamine (TEA), dimethyl sulfoxide (DMSO), acetone, and all other reagents were used as received.

Synthesis of $(PCL)_2(PDEA\text{-}b\text{-}PPEGMA)_2$

$A_2(BC)_2$ miktoarm star polymer $(PCL)_2(PDEA\text{-}b\text{-}PPEGMA)_2$ was synthesized using the difunctional initiator for sequential ROP of ε-CL and continuous ARGET ATRP of DEA and PEGMA. The typical procedure was as follows: First, pentaerythritol bis(2-bromoisobutyrate) $[(OH)_2{-}Br_2]$ was synthesized using pentaerythritol (6.80 g, 0.05 mmol) and TEA (13.89 mL, 0.10 mmol) with twofold 2-bromoisobutyryl bromide (12.36 mL, 0.10 mmol) in THF (150 mL) at room temperature. Then, the synthesis of $(PCL)_2{-}Br_2$ by ROP of ε-CL (6 g) in bulk was carried out using $(OH)_2{-}Br_2$ (0.434 g, 1 mmol) as a difunctional

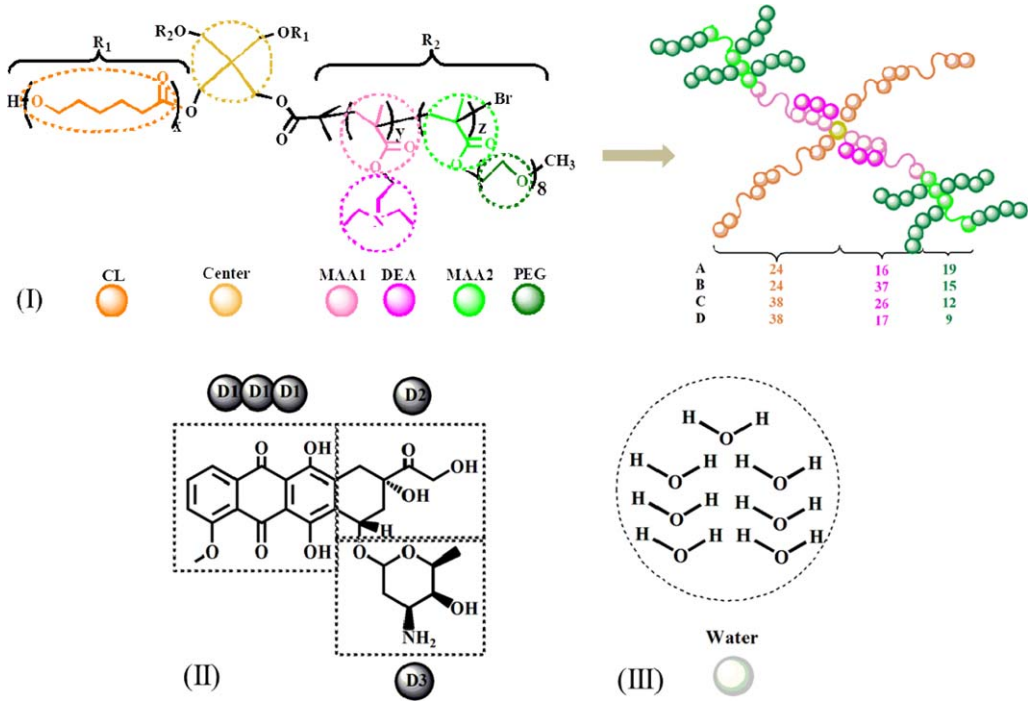

Figure 1. The molecular structures and coarse grain models of (I) polymers (A) $(PCL_{24})_2(PDEA_{16}$-*b*-$PPEGMA_{19})_2$, (B) $(PCL_{24})_2(PDEA_{37}$-*b*-$PPEGMA_{15})_2$, (C) $(PCL_{38})_2(PDEA_{26}$-*b*-$PPEGMA_{11})_2$, and (D) $(PCL_{38})_2(PDEA_{17}$-*b*-$PPEGMA_{9})_2$, (II) DOX, and (III) water.

[Color figure can be viewed in the online issue, which is available at wileyonlinelibrary.com.]

initiator and $Sn(Oct)_2$ (0.1% wt of ε-CL, 0.006 g) as a catalyst at 130°C for 24 h. Finally, $(PCL)_2$(PDEA-*b*-PPEGMA)$_2$ was polymerized in toluene at 70°C using $(PCL)_2$—Br_2 (4.0 g, 0.8 mmol) as macroinitiator *in situ* monitored by ReactIR iC10 (Metter-Toledo AutoChem). The FTIR spectra were collected every minute and the change of absorbance at 938 cm^{-1} [=CH_2 wags of the DEA and PEGMA ($M_n = 475$)] was used to provide the conversion of monomers during the polymerization.[27,28] DEA (4.8 g) was introduced by syringe until the absorbance of 938 cm^{-1} kept almost constant and then the second monomer PEGMA ($M_n = 475$, 6.4 g) was introduced to continue the polymerization. A tiny amount of $CuBr_2$ catalyst (0.0143 g, 0.064 mmol) and ligand HMTETA (0.164 mL, 0.64 mmol) were used together with a sufficiently large excess of reducing agent $Sn(Oct)_2$ (0.259 g, 0.64 mmol).

Critical micellar concentration measurement

The Critical micellar concentration (CMC) values of $(PCL)_2$(PDEA-*b*-PPEGMA)$_2$ were determined by the fluorescence probe technique using pyrene as a fluorescence probe. Pyrene dissolved in acetone was added into deionized water (pH 7.4) to make a concentration of 12×10^{-7} M following by removed acetone 2 h through evaporation. The final concentration of pyrene was adjusted to 6×10^{-7} M. The $(PCL)_2$(PDEA-*b*-PPEGMA)$_2$ (5 mg) was first dissolved into 50 mL deionized water and then diluted to a series of concentrations from 0.0001 to 0.1 mg/mL with deionized water. Then 10 mL of polymer solutions at different concentrations were added to the pyrene filmed vials respectively and the combined solutions were equilibrated at room temperature in dark for 24 h before measurement. The fluorescence excitation spectra of polymer/pyrene solutions were measured and used for determining the CMC values.

Preparation of blank and DOX-loaded micelles

The blank and DOX-loaded $(PCL)_2$(PDEA-*b*-PPEGMA)$_2$ self-assembled micelles were prepared by a membrane dialysis technique. Briefly, DOX·HCl (10 mg or 20 mg) was stirred with double mole TEA in 20 mL of DMSO overnight to obtain a DOX base. The $(PCL)_2$(PDEA-*b*-PPEGMA)$_2$ (40 mg) were dissolved in another 20 mL of DMSO (40 mL for blank micelles) and then mixed with the DOX base solution followed by stirring for 4 h. The mixture solution was transferred to dialysis bag (MWCO = 3.5 kDa) and dialyzed against deionized water for 24 h to remove the organic solvents and free DOX. The deionized water was changed every 4 h for the first 8 h and then replaced every 6 h. After dialysis, the micelles were filtered by a membrane filter (0.45 μm pore) to remove aggregated particles. Then, half of the blank and DOX-loaded micelles were used to study the pH-responsive behavior by the addition of NaOH or HCl (0.01 M) solution. And the remaining blank and DOX-loaded micelles were collected by freeze-drying to obtain dried product. The received white powder was stored at −20°C until further experiments. The values of hydrodynamic diameters (D_hs) and morphologies of the blank and DOX-entrapped micelles were monitored by DLS and TEM. DOX-loaded micelles were dissolved in 10 mL of DMSO under vigorous vortexing and analyzed by UV-VIS spectrophotometer (UV-2450, Shimadzu, Japan) at 480 nm to obtain DOX loading content (LC) and entrapment efficiency (EE), wherein a calibration curve was obtained with DOX-DMSO solutions with different DOX concentrations.

In vitro *DOX release study*

Release profiles of DOX from the DOX-loaded micelles at a concentration of 1 mg/mL were studied in different media

Table 1. Interaction Parameters a_{ij} Used in the Simulation

	DEAH	DEA	CL	Center	D1	D2	D3	MAA1	MAA2	PEG	Water
DEAH	25.00										
DEA	11.87	25.00									
CL	96.82	25.95	25.00								
Center	27.39	25.83	28.38	25.00							
D1	81.77	23.72	23.45	31.06	25.00						
D2	87.04	24.25	23.23	29.20	25.26	25.00					
D3	85.25	25.29	24.77	28.45	25.09	25.05	25.00				
MAA1	17.14	30.44	27.01	34.35	25.63	21.63	24.12	25.00			
MAA2	17.14	30.44	27.01	34.35	25.63	21.63	24.12	25.00	25.00		
PEG	20.82	45.79	37.10	53.24	25.31	24.22	25.34	28.48	28.48	25.00	
Water	11.35	37.28	53.20	81.94	43.70	27.03	23.74	34.60	34.60	26.10	25.00

(pH 5.0, pH 6.5, and pH 7.4). Briefly, 5 mg of DOX-loaded micelles were dispersed in 5 mL different media, and then placed in preswollen cellulose membrane bags (MWCO = 3.5 kDa). The whole bags were placed into 40 mL different media with constant shaking (100 rpm) at 37°C (Dissolution Tester RCZ-8B, TDTF, China). The samples were drawn at predetermined time intervals and the concentrations of released DOX were monitored by UV-VIS spectrophotometer at 480 nm. Each experiment was done in triple.

Characterization

^{1}H NMR spectra measurements were examined in $CDCl_3$ at 25°C using Bruker AVANCE III 400 operating at 400 MHz. The number average molecular weight (M_n) and polydispersity index (M_w/M_n) were determined by gel permeation chromatography (GPC) adopting an Agilent 1200 series GPC system equipped with a LC quant pump, PL gel 5 mm 500 Å, 10^4 Å, and 10^5 Å columns in series, and RI detector. The column system was calibrated with a set of monodisperse polystyrene standards using HPLC grade THF as mobile phase with a flow rate of 1.0 mL/min at 30°C. Fluorescence spectra were recorded using a fluorescence spectrophotometer (F-4500, Hitachi, Japan). The hydrodynamic diameter (D_h) and distribution (PDI) of micelles were measured by DLS (Malvern Zetasizer Nano S, UK). Morphologies of micelles were investigated by TEM (Hitachi H-7650, Japan) operating at 80 kV.

Simulation Method

Simulation method and models

DPD simulation is based on the coarse grain models of all the contents in the investigated system. In this method, a set of soft interacting particles called beads represent groups of several atoms or volumes of fluid. The force between each pair of beads is a sum of a conservative force ($\mathbf{F}_{ij}^{C}$), a dissipative force ($\mathbf{F}_{ij}^{D}$), and a random force ($\mathbf{F}_{ij}^{R}$).[29] These forces ensure that DPD method effectively stretches the characteristic time scale of the simulated system compared to the full atomistic and molecular dynamic simulation.[30,31] Additionally, by establishing a relationship between a simple function form of the conservative repulsion in DPD and the Flory–Huggins parameter theory, DPD method has been widely applied in the study of mesoscale structures of complex systems.[32–34]

In these coarse grain models shown in Figure 1, the molecular structure of DOX was divided into three types of beads (D1, D2, and D3), which were shown in black color. Seven water molecules were represented as one bead (Water). In neutral system, the polymers were divided into six types of beads, whose names and colors were center (neopentane)-yellow, CL (caprolactone)-orange, MAA1-pink, MAA2-bright green, DEA-rose pink, and PEG-dark green, respectively. In acidic system, the pH-sensitive DEA is ionized and represented by DEAH. MAA1 and DEA were divided from 2-(diethylamino) ethyl methacrylate (PDEA); MAA2 and PEG were divided from PPEGMA. The mass and radius of each bead were 112 amu and 3.7 Å, and the cut-off radius r_c between two beads was 8.6 Å. The corresponding topology structures of the coarse grain models of the polymers were shown in Figure 1I. The number of different beads for the four polymeric molecules stated in Figure 1I on the right was dependent on the components of the polymers in the experiments, assuring each chain length of the coarse grain models of the polymers was consistent with those of the polymers in the experiments. Besides, considering that the values of the spring constant in the range of 2.0 to 4.0 (reduced) have been found to give reasonable results in most circumstances and 4.0 is widely used in many DPD works, the spring constant was set to 4.0 in our simulations, resulting in a slightly smaller distance for bonded beads than for non-bonded ones. And the bead density was 3 used in this work, namely a cube of r_c^3 contained three beads.[5,17]

Interaction parameters

According to the coarse-grained models for the four polymeric molecules, DOX and water molecules, we carried out molecular dynamics simulation on the pure and binary components as listed in Table 1 to obtain Flory–Huggins parameters. The COMPASS force field was applied on all the components. Either pure or binary mixture system was constructed by the Amorphous Cell module in Materials Studio 5.5 (Accelrys). It should be noted that in the acidic environment the tertiary amine groups of PDEA are protonated (DEAH). To electrically neutralize the positive charges on DEAH, the same amount of chloride ions was presented in the system. The interaction repulsion a_{ij} between bead i and j depending on the underlying atomistic interaction is linearly related to the Flory–Huggins parameters (χ_{ij}) as given in Eq. 1[35–37]

$$a_{ij} = a_{ii} + 3.27\chi_{ij} \quad (1)$$

where a_{ii} is equal to 25. For binary components i and j, the Flory–Huggins parameter χ_{ij} can be estimated by Eq. 2[38]

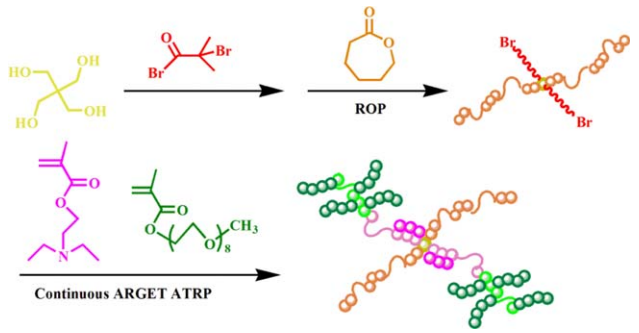

Figure 2. Schematic description of the synthesis of $(PCL)_2(PDEA\text{-}b\text{-}PPEGMA)_2$.

[Color figure can be viewed in the online issue, which is available at wileyonlinelibrary.com.]

$$\chi_{ij} = \frac{\Delta E_{\text{mix}} V_{\text{r}}}{RT \varphi_i \varphi_j V} \tag{2}$$

where R is the gas constant and T is temperature; φ_i and φ_j are the volume fractions of components i and j, respectively; V is total volume and V_{r} is reference volume; ΔE_{mix} is the mixing energy of the binary components, which is obtained by the potential energy of the binary mixture, potential energies of pure components i and j, respectively.

In the case of the nonpolar components or components without specific interactions (e.g., hydrogen bonding), and if the excess entropy and excess volume can be ignored, χ_{ij} can be obtained from the solubility parameters[39,40]

$$\chi_{ij} = \frac{(\delta_i - \delta_j)^2 V_r}{RT} \tag{3}$$

where δ_i and δ_j are the solubility parameters of components i and j, respectively, which are calculated by molecular dynamics simulations using the Amorphous Cell and Discover modules in the same software. Herein, the Flory–Huggins parameters of the pairs with strong hydrophobicity, such as Center-CL/D1/D2/D3/MAA1/MAA2, CL-DEA/MAA1/MAA2, D1-D2/D3/MAA1/MAA2, and D2-D3 were computed by Eq. 3, while the other pairs with stronger polarity were computed by Eq. 2.

Simulation conditions

In the studies, DPD simulations were used in two systems: the neutral system (pH 7.4) and acidic system (pH 6.5, 5.0). These systems consist of water, the four polymeric molecules, and DOX. The neutral system was mainly conducted to study the formation of drug-loaded micelles and the distribution of DOX in the micelles. In acidic systems, we further discussed the pH responsive characteristics on drug-loaded micelles. This part of simulation was performed in the Mesocite module of Materials Studio 5.5 software. A cubic simulation box with periodic boundary condition was applied in all directions. Rectangular simulation boxes of 250 × 250 × 250 $Å^3$ were used. The results shown in Supporting Information Fig. S2 to S4 confirmed that the obtained micelles from the systems in boxes of 250 × 250 × 250 $Å^3$ with different initial configurations (different initial particle positions and random initial velocities) were structurally similar, indicating that the simulation results of the study are repeatable and conclusive. Moreover, simulation boxes of 250 × 250 × 250 $Å^3$ is sufficient to avoid the finite size effects according to Supporting Information Fig. S5 and S6 that the structures and the DOX distributions of the micelles were similar in the boxes of different sizes (200 × 200 × 200, 250 × 250 × 250, 300 × 300 × 300, 350 × 350 × 350, and 400 × 400 × 400 $Å^3$) at the same density. As each polymer has different components, different simulation steps were used in different systems to obtain equilibrium. According to our investigation, the minimum simulation steps applied to the polymer with more hydrophobic component was 250,000, which was decided after we lengthened the simulation steps and found out the structure of the micelles did not show any changes. To get more close to the experiment results, the concentrations of the polymers and DOX in the simulation systems were consistent with those of the experiment systems: the experimental concentrations of the four polymers were 40 mg in each system, correspondingly the simulation concentrations of the four polymers were set to 5.26%, 5.25%, 5.11%, and 5.04% respectively, which were calculated from the molecular weight and volume of the polymers as well as the density of the systems. Similarly, the simulation concentrations of DOX were set to 0.46%, 0.91%, 1.37%, and 1.83% in accordance with the concentrations of 5, 10, 15, and 20 mg in the experimental cases. To investigate the pH sensitivity of the drug-loaded micelles, the pH values of the system were given in two cases: pH 6.5 and pH 5.0 with the same components, which were also consistent with the experiments. The protonation degree of the pH-sensitive groups relates to the intrinsic pK_a value and the pH values of the exterior environment, whose value is given by the Henderson–Hasselbalch formula.[41] According to the formula, when the pH values of the solvents are 6.5 and 5.0, there are around 72% and 100% DEA groups protonated, respectively.

Results and Discussion

Synthesis and characterization of $(PCL)_2(PDEA\text{-}b\text{-}PPEGMA)_2$

The miktoarm star polymers $(PCL)_2(PDEA\text{-}b\text{-}PPEGMA)_2$ were synthesized using the difunctional initiator for sequential ROP of ε-CL and continuous ARGET ATRP of DEA and PEGMA *in situ* monitored by ReactIR iC10, as

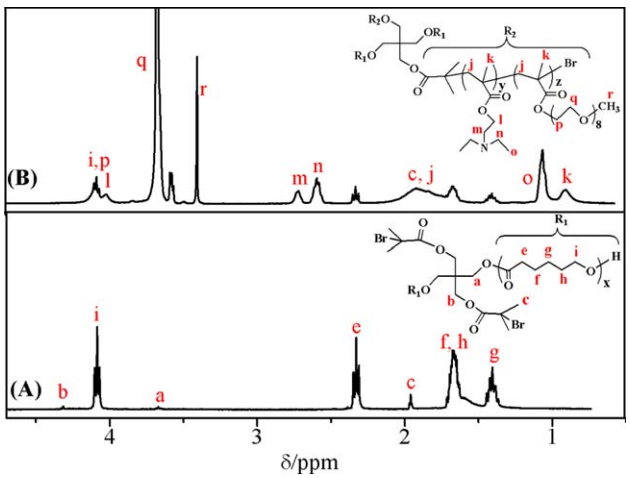

Figure 3. ^1H NMR spectra of $(PCL)_2\text{-}Br_2$ (A) and $(PCL)_2(PDEA\text{-}b\text{-}PPEGMA)_2$ (B) in $CDCl_3$.

[Color figure can be viewed in the online issue, which is available at wileyonlinelibrary.com.]

Table 2. GPC, ^{1}H NMR, and CMC Data of $(PCL)_2(PDEA\text{-}b\text{-}PPEGMA)_2$

Sample	$M_{n,\ GPC}$[a]	M_w/M_n[a]	x[b]	y[b]	z[b]	$M_{n,\ NMR}$[c]	$M_{n,\ RealIR}$[d]	CMC (mg/L)[e]
$(PCL_{24})_2(PDEA_{16}\text{-}b\text{-}PPEGMA_{19})_2$	14,888	1.28	24.22	15.86	18.73	29,617	28,200	4.3
$(PCL_{24})_2(PDEA_{37}\text{-}b\text{PPEGMA}_{15})_2$	12,692	1.19	24.22	37.18	15.02	33,977	34,300	3.0
$(PCL_{38})_2(PDEA_{26}\text{-}b\text{-}PPEGMA_{11})_2$	18,302	1.19	38.24	25.62	11.47	29,530	28,524	2.8
$(PCL_{38})_2(PDEA_{17}\text{-}b\text{-}PPEGMA_{9})_2$	13,586	1.35	38.24	17.21	9.43	24,480	24,614	2.4

[a]Measured by GPC in THF.
[b]The subscripts were the degree of polymerization of PCL (x), PDEA (y), and PPEGMA (z) calculated from ^{1}H NMR spectra.
[c]Calculated by the equations $M_{n,NMR} = (114 \times x + 185 \times y + 475 \times z) \times 2 + 434$.
[d]Calculated by monomer conversion from the ReactIR.
[e]Determined by a fluorescence spectroscopic method.

illustrated in Figure 2. Representative ^{1}H NMR spectra of $(PCL)_2$—Br_2 and $(PCL)_2(PDEA\text{-}b\text{-}PPEGMA)_2$ were depicted in Figure 3 and all of the peaks corresponding to characteristic hydrogen atoms were labeled, demonstrating that $(PCL)_2(PDEA\text{-}b\text{-}PPEGMA)_2$ had been successfully synthesized and characterized. The degree of polymerization of PCL (x), PDEA (y), and PPEGMA (z) and the molecular weights ($M_{n,NMR}$) were calculated from the integration ratio values of signal (g) to (a) (I_g/I_a), signal (n) to (g) (I_n/I_g), and signal (r) to (g) (I_r/I_g), respectively, as summarized in Table 2. From the change of absorbance at 938 cm^{-1} *in situ* monitored by react infrared spectroscopy, the conversions of DEA and PEGMA could be calculated during the ARGET ATRP. Thus, the molecular weights ($M_{n,ReactIR}$) of $(PCL)_2(PDEA\text{-}b\text{-}PPEGMA)_2$ could be calculated from the conversions of DEA and PEGMA, which has seldom been reported before. The $M_{n,ReactIR}$ listed in Table 2 were in good accord with the $M_{n,NMR}$, suggesting that $(PCL)_2(PDEA\text{-}b\text{-}PPEGMA)_2$ with different PCL/PDEA/PPEGMA contents were well defined. GPC results listed in Table 2 appeared monomodal symmetric distribution, indicating well-controlled process of ROP and the continuous ARGET ATRP of DEA and PEGMA. The values of M_w/M_n were below 1.40, which are acceptable for further application of delivering drugs. It was also found that GPC analysis for $(PCL)_2(PDEA\text{-}b\text{-}PPEGMA)_2$ tended to underestimate the molecular weight (which was typically smaller than $M_{n,NMR}$) as compared to their linear counterpart due to the reduced hydrodynamic volumes.[42,43]

The formation of micelles self-assembled from four $(PCL)_2(PDEA\text{-}b\text{-}PPEGMA)_2$ with different block ratios in aqueous phase was verified using a fluorescence technique with pyrene as a fluorescence probe.[44–46] A lower CMC value is desirable for increasing micelle stability in the blood stream. The CMC values were determined from the threshold concentration, where the intensity ratio I_{339}/I_{336} begins to increase markedly. The CMC values have difference because of the four different block ratios of polymers. As shown in Table 2 and Supporting Information Figure S1, the CMC values of $(PCL)_2(PDEA\text{-}b\text{-}PPEGMA)_2$ of four topological structures were in the range of 0.0024–0.0043 mg/mL, decreasing as the weight fraction of PCL and PDEA increased.[47]

pH-responsive self-assembly behavior of $(PCL)_2(PDEA\text{-}b\text{-}PPEGMA)_2$

To discuss the effect of different polymeric structures on the micellar structures at varying pH values, transmittance of four blank $(PCL)_2(PDEA\text{-}b\text{-}PPEGMA)_2$ micelles with different block ratios, which reflects structural transformation of the micelles, was characterized by UV-VIS spectrophotometer at different pH values (pH 8.0, 7.4, 6.5, and 5.0) at 500 nm. As shown in Figure 4, at pH 8.0, the transmittance values of the four micelles were relative low with around 52%–83%. The reason is that the PDEA segments were deprotonated and the PDEA chains shrank completely to compose the micellar core with PCL, which formed compact micellar structures. By decreasing the pH values from 8 to 5, the light transmittance of the micelle solutions appeared obvious fluctuation, which indicated that the PDEA chains were gradually protonated in acid aqueous solution, resulting in the increase of hydrophilicity of the micellar core and transmittance of the micelle solutions. The increased transmittance value of $(PCL_{24})_2(PDEA_{37}\text{-}b\text{-}PPEGMA_{15})_2$ micelles with longest PDEA block was 43%, which was the most obvious among the four micelles. On the contrary, the increased transmittance value of $(PCL_{24})_2(PDEA_{16}\text{-}b\text{-}PPEGMA_{19})_2$ micelles was 13% as the PDEA block is shorter. We also carried out DPD simulations on the micelles at pH 5.0, the morphologies of which were shown in Figure 5. We could see that the PDEA chains of the polymers were extended and loose at pH 5.0, making the chains apart from each other. The light went through the micelles more easily and thus resulted in the increase of the transmittance. Besides, the micelles with more PDEA and PEG blocks had looser structures and contained a smaller hydrophobic core in acidic condition (e.g., Figures 7B, C), which are in favor of the transmission. Therefore, the micellar core owned the stronger hydrophilicity at pH 5.0, whose transmittance values

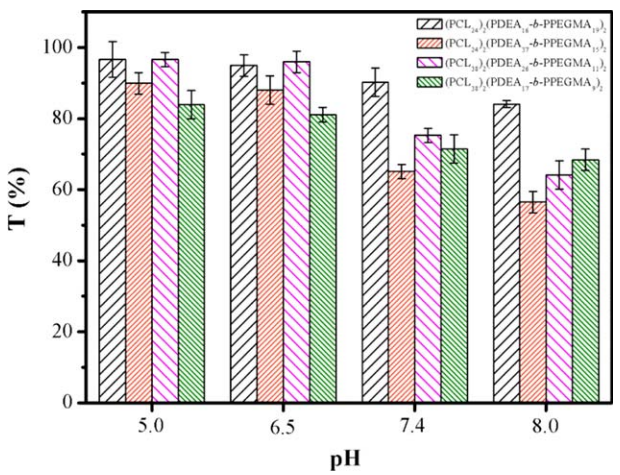

Figure 4. Effect of pH values on the transmittance (*T*%) at 500 nm of $(PCL)_2(PDEA\text{-}b\text{-}PPEGMA)_2$ micelles at different concentrations in aqueous solution.

[Color figure can be viewed in the online issue, which is available at wileyonlinelibrary.com.]

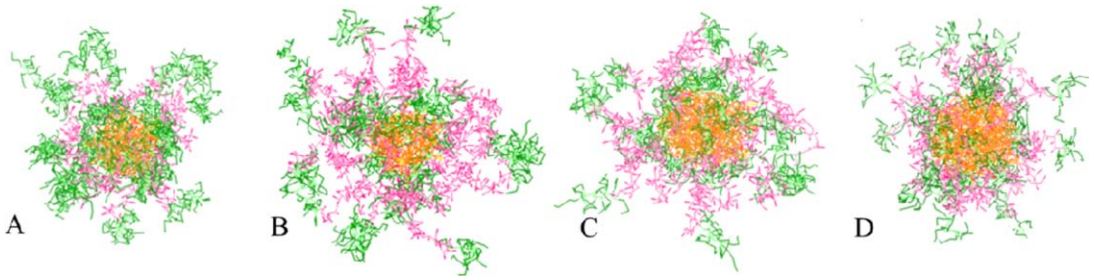

Figure 5. Typical simulated section views of blank micelles at pH 5.0 (A) $(PCL_{24})_2(PDEA_{16}$-*b*-$PPEGMA_{19})_2$, (B) $(PCL_{24})_2(PDEA_{37}$-*b*-$PPEGMA_{15})_2$, (C) $(PCL_{38})_2(PDEA_{26}$-*b*-$PPEGMA_{11})_2$, and (D) $(PCL_{38})_2(PDEA_{17}$-*b*-$PPEGMA_9)_2$.

[Color figure can be viewed in the online issue, which is available at wileyonlinelibrary.com.]

of four micelles were 97%, 90%, 97%, and 84%, respectively.

As can be seen from the above discussion of transmittance and DPD simulations, different polymeric structures also play key role in the D_hs of the micelles from the facile pH adjusting. Figure 6 obtained from DLS measurement showed that, at pH 8.0, both micelles were in a compact, collapsed form because the PDEA segments were deprotonated with the D_hs remained almost constant, the values of which were around 57–72 nm. When decreasing pH from 8 to 5, the tertiary amine groups of PDEA were gradually protonated and the increasing hydrophilicity of PDEA resulted in the stretching of the polymer chains and the swelling of the micelles. In addition, the electrostatic repulsion between the PDEA chains also promoted the micelles swelling. As a result, the D_hs of the micelles were observed significant increase. In the case of pH 5.0, the D_hs values were around 96–121 nm. And D_h was 121 nm for $(PCL_{24})_2(PDEA_{37}$-*b*-$PPEGMA_{15})_2$ micelles with the highest weight fraction of PCL and PDEA.

To further validate the pH-induced changes on the D_hs of the micelles after protonation, the radius of gyration of the PDEA chains of the polymeric micelles before and after protonation (pH 5.0), were calculated in our DPD simulation. The radius of gyration is defined as the root mean square distance of the beads in the micelles from their common center of mass, reflecting the extended degree of the chains in the space in the simulation. It turned out that the radius of gyration (All dimensional values shown below were given in DPD units) of the PDEA chains of the micelles in pH 5.0 increased by 15.5% ($(PCL_{24})_2(PDEA_{16}$-*b*-$PPEGMA_{19})_2$: from 174 to 201), 46.5% ($(PCL_{24})_2(PDEA_{37}$-*b*-$PPEGMA_{15})_2$: from 258 to 378), 25.8% ($(PCL_{38})_2(PDEA_{26}$-*b*-$PPEGMA_{11})_2$: from 279 to 351) and 20.3% ($(PCL_{38})_2(PDEA_{17}$-*b*-$PPEGMA_9)_2$: from 192 to 231). As a result, the radius of gyration of the protonated PDEA chains for the four polymeric micelles increased after protonation. The radius of gyration of the PDEA chains of the micelles which contained more PDEA contents was larger than those with shorter PDEA contents and showed a more outstanding growth rate. $(PCL_{24})_2(PDEA_{37}$-*b*-$PPEGMA_{15})_2$ showed the largest size, followed by $(PCL_{38})_2(PDEA_{26}$-*b*-$PPEGMA_{11})_2$, $(PCL_{38})_2(PDEA_{17}$-*b*-$PPEGMA_9)_2$, and $(PCL_{24})_2(PDEA_{16}$-*b*-$PPEGMA_{19})_2$), which was in agreement with the D_hs shown in Figure 6, suggesting the increase on the radius of gyration of the pH-sensitive chains, in other words, the ratio of the pH-sensitive block may be an important factor inducing the change on the size of micelles.

As mentioned above, the effect of the pH on the D_h values of the micelles was attributed to the swelling of the micelles resulting from the increased hydrophility caused by the protonation of amine groups. The TEM images of the micelles also verified the structural transformation of the micelles from a compact state to a swollen state as the pH decreased. However, the detailed microscopic structures of the micelles cannot be reflected from the TEM images (Figure 7I). Herein, we performed DPD simulations on the micelles to have a deeper insight into the corresponding structures of the micelles in the experiment systems. $(PCL_{24})_2(PDEA_{37}$-*b*-$PPEGMA_{15})_2$ was set as an example at pH 7.4, 6.5, and 5.0, which were shown in the Figure 7II. The simulation images of the micelles were in good agreement with those in the TEM, demonstrating that the spiky shelled and the loose structure of the micelles are generated from the stretch of the protonated PDEAH chains.

For further discussion on the microstructure of the polymeric micelles in acidic condition, the radial distribution function (RDF) was used to analyze the distribution of polymer blocks as well as drug particles in the micelles. The RDF is defined as

$$g_{ij}(r) = \frac{\langle \Delta N_{ij}(r \rightarrow r+\Delta r) \rangle V}{4\pi r^2 \Delta r N_i N_j} \tag{4}$$

where $\langle \Delta N_{ij}(r \rightarrow r+\Delta r) \rangle$ is the ensemble averaged number of bead j around bead i within the volume of a shell from r

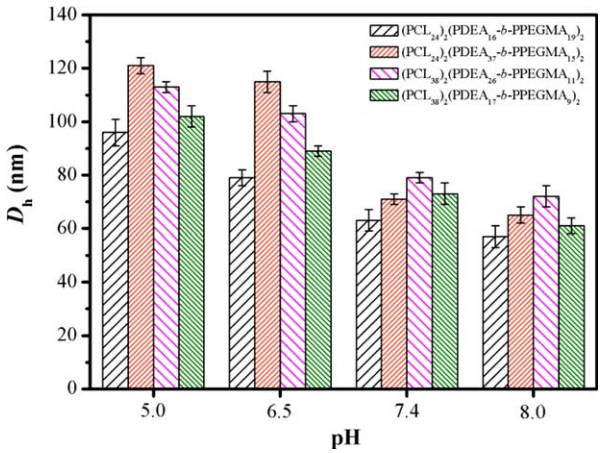

Figure 6. Effect of pH values on the D_hs of $(PCL)_2(PDEA$-*b*-$PPEGMA)_2$ micelles at different concentrations in aqueous solution.

[Color figure can be viewed in the online issue, which is available at wileyonlinelibrary.com.]

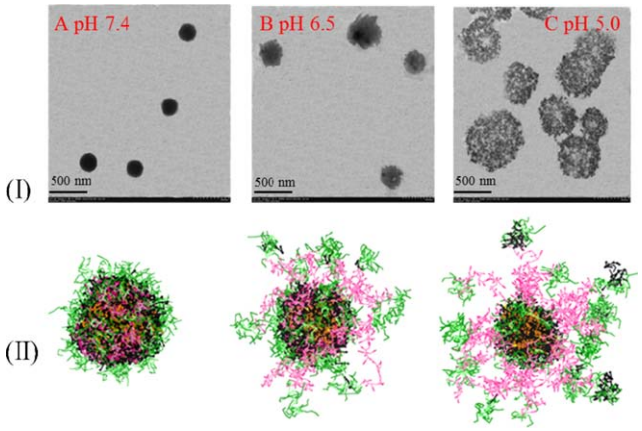

Figure 7. TEM images (I) and typical simulated section views (II) of DOX-loaded $(PCL_{24})_2(PDEA_{37}$-*b*-$PPEGMA_{15})_2$ micelles at different pH conditions: (A) pH 7.4, (B) pH 6.5, and (C) pH 5.0.

[Color figure can be viewed in the online issue, which is available at wileyonlinelibrary.com.]

to $r+\Delta r$, V is the volume of the system, N_i and N_j represent the numbers of bead i and j, respectively.[38] Herein, the RDF curves between CL (CL was used as a reference here, regarded as the core of the micelles) and DEA, PEG, as well as DOX of the four polymeric micelles were acquired before and after protonation as shown in Figure 8, demonstrating the distribution of different contents in the micelles in neutral and acidic environments. $g(r)$ shown in Figure 10 is the distribution function, and r values correspond to the peaks of RDF curve reflect the distance between two kinds of beads. Set CL and DEA beads for instance, the highest peak represents that most of the CL beads appear in the corresponding distance away from DEA beads. The relative position r between different beads reflects the attraction between different types of beads.

According to the RDF results, there was a big difference between the CL-DEA curves before and after protonation, and all the four polymeric micelles had the similar trend, thus we chose the RDF of $(PCL_{24})_2(PDEA_{37}$-*b*-$PPEGMA_{15})_2$ micelles as an example. Before protonation, the CL-DEA curves exhibited a sharp peak, indicating that PDEA chains are mainly distributed in the region near the PCL core, which reflects the structural characteristic that PDEA form the middle layer of the micelles in the neutral condition. In the case of protonation, the curve of CL-DEA was similar to that of PEG-DEA without a sharp peak, suggesting that PDEA chains are distributed in the area far away from the PCL core, which reflects the structural characteristic that the PDEA chains are extended to the exterior of the micelles due to their strong hydrophilicity when protonated.

The trend of the RDF curves of CL-DOX were similar to that of CL-DEA, indicating that DOX and PDEA are almost in the same region of the micelles, in other words, the quantity of DOX distributed in the area formed by DEA groups is considerably large. The results also reflect the compatibility between different components. According to the interaction parameters shown in Table 1, PCL has the best compatibility with the DOX molecules (23.23–24.77), whose interaction parameters were smaller than that of PCL chains (23.72–25.29). However, a large repulsion generates between PDEA chains and DOX molecules after protonation (81.77–87.04), which was shown in Figure 8, means that the RDF curve of DOX and PDEA separated from each other.

Combining the experiment and simulation results analyzed above, it can illustrate that with the decrease of pH, PDEA was protonated progressively, that the amine groups of the polymers are protonated to form cationic NH_3^+ groups. The rapid increase on the hydrophilicity of the PDEA chains leads to their transformation from a curling shape to a divergent extended shape, which can be observed from the DPD simulations, and the micelles got swollen as the chains stretched to the solvent. Besides, as the PDEAH chains were with the strong positive charges, the electrostatic repulsion between the chains also promotes the swelling of the micelles. Thus, the results in the changes of D_hs and transmittance of the micelles in acidic environments can be observed.

The effect of polymeric structures on drug loading capacity

Entrapping these polymers with 10 or 20 mg DOX induced obvious increases in size of micelles, which were approximately 40 or 50 nm comparing with blank micelles, as shown in Table 3. The LC increased with the increase of fed drug while the EE decreased for relative saturated capacity of solubilizing DOX in the micellar core. And the copolymer micelles at the same drug/polymer ratio with longer length of PCL and PDEA block exhibited an enhanced drug entrapping ability. For example, the LC values of $(PCL_{24})_2(PDEA_{16}$-*b*-$PPEGMA_{19})_2$, $(PCL_{24})_2(PDEA_{37}$-*b*-$PPEGMA_{15})_2$, and $(PCL_{38})_2(PDEA_{17}$-*b*-$PPEGMA_9)_2$ were 9.0%, 11.6%, and 15.7% as increasing the weight fraction of PCL and PDEA. In this work, the maximum LC and EE of DOX belonged to $(PCL_{38})_2(PDEA_{17}$-*b*-$PPEGMA_9)_2$ was calculated to be 19% and 74.49%, respectively.

To discuss the structural characteristic and drug-loaded properties of different assembled micelles, the DOX distribution and capacity of the micelles were obtained by DPD simulations. Compared to the experimental systems, two

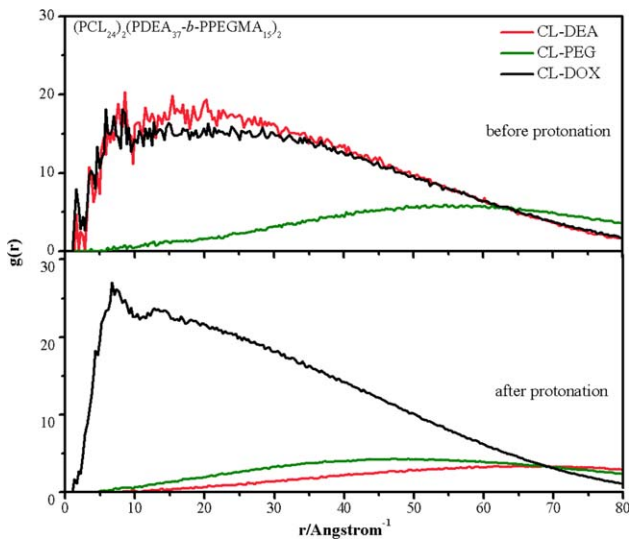

Figure 8. RDF profiles of $(PCL_{24})_2(PDEA_{37}$-*b*-$PPEGMA_{15})_2$ before and after protonation.

[Color figure can be viewed in the online issue, which is available at wileyonlinelibrary.com.]

Table 3. Properties of DOX-Loaded $(PCL)_2(PDEA\text{-}b\text{-}PPEGMA)_2$ Micelles

	DOX-Loaded Micelles (10 mg)				DOX-Loaded Micelles (20 mg)			
Entry[a]	D_h (nm)[b]	PDI[b]	LC(%)[c]	EE(%)[c]	D_h (nm) [b]	PDI[b]	LC(%)[c]	EE(%)[c]
$(PCL_{24})_2(PDEA_{16}\text{-}b\text{-}PPEGMA_{19})_2$	103	0.047	9.0	39.56	114	0.254	11.8	26.76
$(PCL_{24})_2(PDEA_{37}\text{-}b\text{-}PPEGMA_{15})_2$	108	0.313	11.6	52.49	129	0.139	14.5	33.92
$(PCL_{38})_2(PDEA_{26}\text{-}b\text{-}PPEGMA_{11})_2$	123	0.253	12.1	55.06	165	0.283	17.5	42.42
$(PCL_{38})_2(PDEA_{17}\text{-}b\text{-}PPEGMA_{9})_2$	108	0.384	15.7	74.49	143	0.075	19.0	46.91

[a]The same entry as Table 2.
[b]Determined by DLS.
[c]Determined by UV–VIS spectrophotometer.

systems with 5 mg/40 mg and 15 mg/40 mg DOX/polymer concentration ratios were added to find the regularity, the simulation results are shown in Figure 9. Figure 9II was obtained based on the simulation models in Figure 9I. As the RDF curves of the four polymeric micelles appeared to be similar, only the results of $(PCL_{24})_2(PDEA_{16}\text{-}b\text{-}PPEGMA_{19})_2$

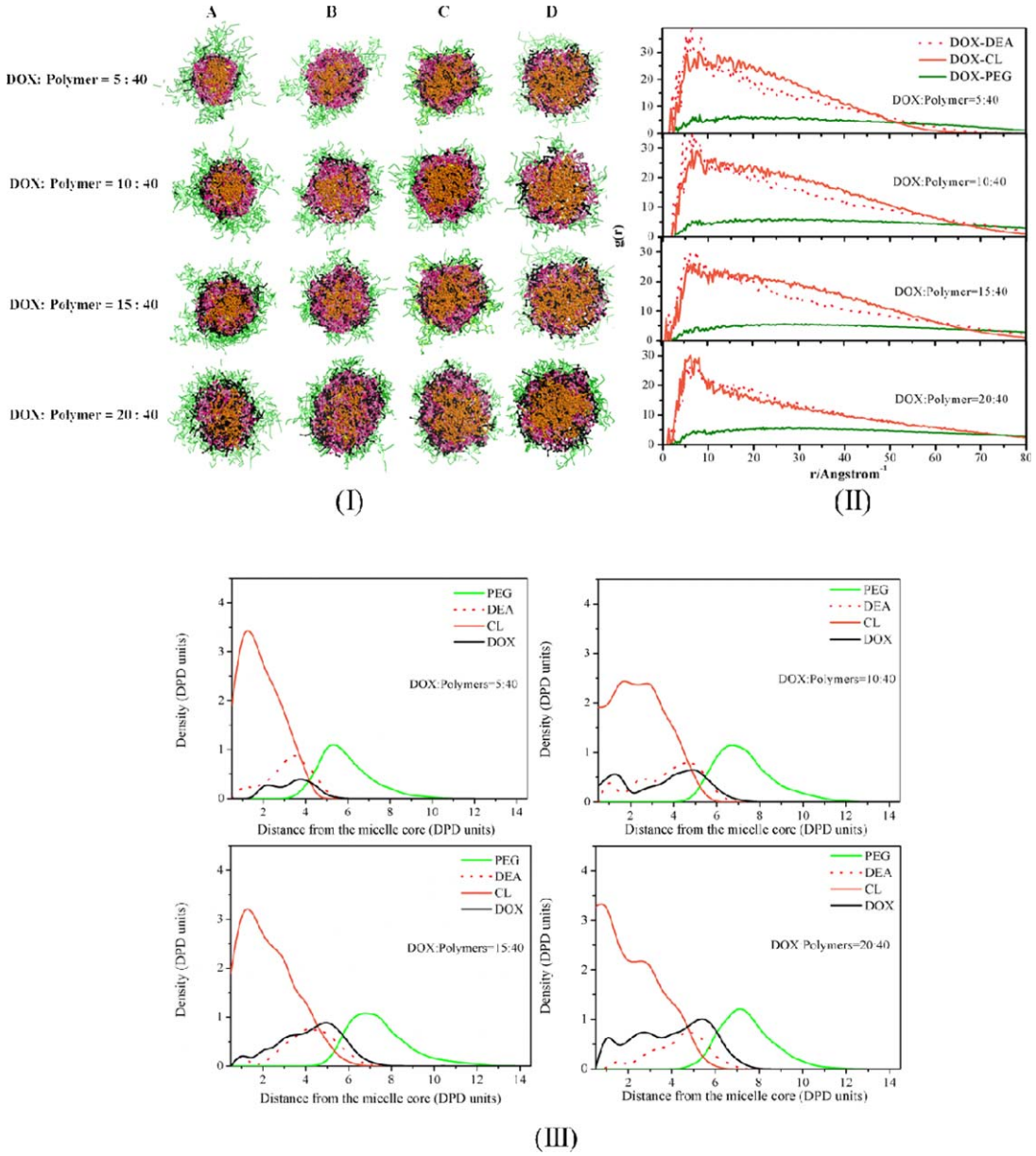

Figure 9. (I) Cross-section views of the polymeric micelles with different DOX concentrations (A) $(PCL_{24})_2(PDEA_{16}\text{-}b\text{-}PPEGMA_{19})_2$, (B) $(PCL_{24})_2(PDEA_{37}\text{-}b\text{-}PPEGMA_{15})_2$, (C) $(PCL_{38})_2(PDEA_{26}\text{-}b\text{-}PPEGMA_{11})_2$, and (D) $(PCL_{38})_2(PDEA_{17}\text{-}b\text{-}PPEGMA_{9})_2$. (II) The RDF and (III) density profiles of different beads of the $(PCL_{24})_2(PDEA_{16}\text{-}b\text{-}PPEGMA_{19})_2$ micelles with different DOX concentrations.

[Color figure can be viewed in the online issue, which is available at wileyonlinelibrary.com.]

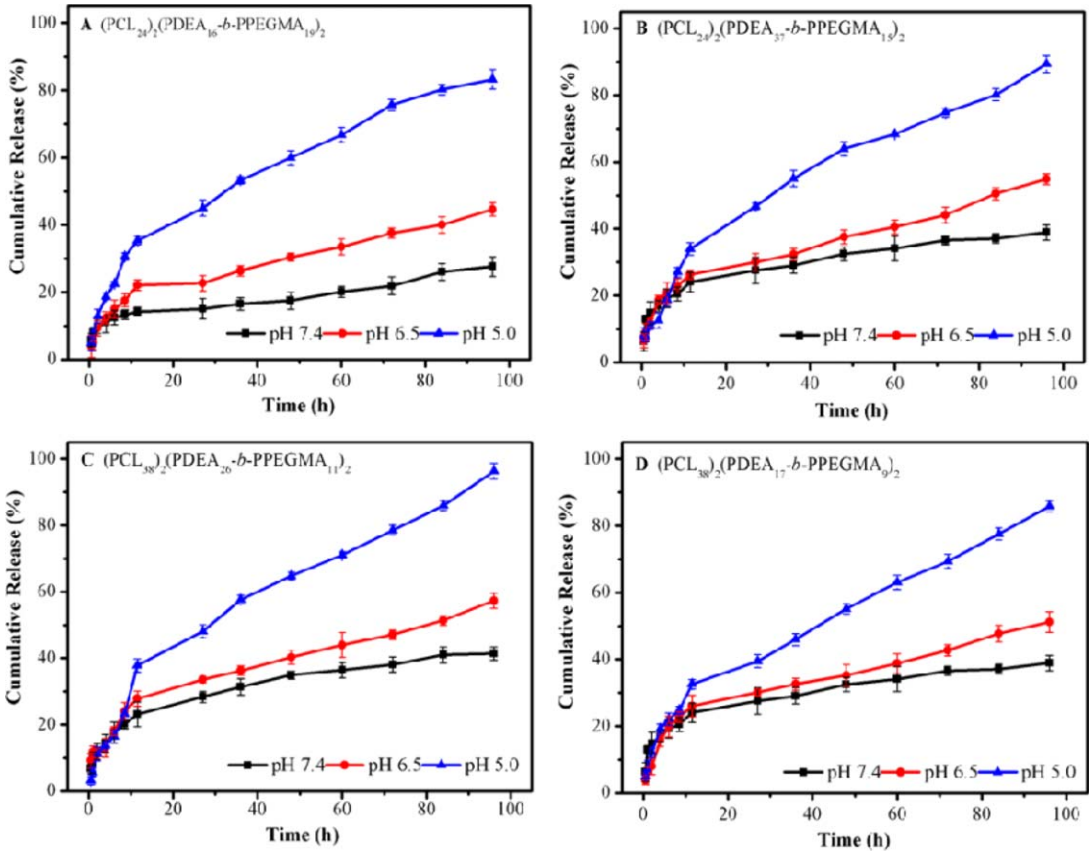

Figure 10. *In vitro* drug release profiles of and DOX-loaded micelles at pH 7.4, pH 6.5 and pH 5.0.

[Color figure can be viewed in the online issue, which is available at wileyonlinelibrary.com.]

micelles were given for the following analysis. The DPD results showed the microstructures of the micelles formed by different polymers: all the micelles presented a core-mesosphere-shell three-layer structure. The PPEGMA chains formed the shell, equivalent to a hydrophilic protective layer of the micelles, sustaining the stability of the micelles. The PDEA chains formed the mesosphere of the micelles, playing a role in pH response together with a drug package effect. The PCL formed the inner core, which also showed a drug package effect. Furthermore, the distribution of DOX can be discussed according to Figure 9. For the micelles loading with a low concentration of DOX in Figure 9I, DOX preferentially distributed in the mesosphere formed by PDEA. The RDF results in Figure 9II also showed that the peak of the DOX-DEA curve was more evident than that of the DOX-CL curve, which meant more DOX molecules distribute in the PDEA area. Because, the DOX molecules need to overcome the space resistance in the process of the diffusion into the inner core of micelles. As the concentration of DOX increased, DOX diffused into the inner core after the area of PDEA is almost saturated, and thus more DOX can be observed in the core area of Figure 9I. It is reflected in Figure 9II that as the DOX increased, the curves of DOX-CL and DOX-DEA got closer and showed an overlapping trend, suggesting the amount of drugs distributed in the inner core increased gradually. For a more direct insight on the distribution of the drugs in the micelles as their concentrations gradually increased, the density profiles of different beads of the $(PCL_{24})2(PDEA_{16}$-*b*-$PPEGMA_{19})_2$ micelles with different DOX concentrations were also given, as shown in Figure 9 (III). The change of DOX distributions reflected in Figure 9 (III) also illustrated that when the drug concentration was in a low level, DOX tended to distribute in the PDEA area (DOX: polymers = 5:40). With the increase of the drug concentration, more DOX molecules distributed inside the core of the micelles (DOX: polymers = 10:40, 15:40 and 20:40). However, the narrow peak at around 5 DPD unit of drug density distribution inside the micelles when DOX: polymers was 20:40 also indicated the middle drug layer between the core and shell of the micelles, which may suggest that it becomes harder for the drugs to diffuse into the core of micelles when they reach a certain concentration range.

As the ratios of components in the four polymers are different, the structures of the micelles are diverse. According to the EE of the micelles determined in the experiment, the capacity of DOX become higher as the hydrophobic chains of the polymers get longer. The experimental results also demonstrated that the EE of $(PCL_{38})_2(PDEA_{17}$-*b*-$PPEGMA_9)_2$ micelles was maximum, while the EE of $(PCL_{24})_2(PDEA_{16}$-*b*-$PPEGMA_{19})_2$ micelles appeared a minimum value, which can be explained via the simulation results of the micellar structures. Because the proportion of hydrophilic PPEGMA in $(PCL_{24})_2(PDEA_{16}$-*b*-$PPEGMA_{19})_2$ is highest, the denser and thicker shell are in favor of the stability of the micelles. In the meanwhile, the LC decreases due to the low proportion of the hydrophobic blocks. For $(PCL_{24})_2(PDEA_{37}$-*b*-$PPEGMA_{15})_2$ with the longest PDEA blocks, their micelles from the cross-section views possess a considerably thick mesosphere, which PDEA section (shown

in pink color) is relatively large, thus their pH-sensitivity is prominent. Moreover, the micelles also presented a good DOX loading capacity due to the good compatibility between DOX and PDEA. The $(PCL_{38})_2(PDEA_{26}$-*b*-$PPEGMA_{11})_2$ micelles may be relatively unstable as the proportion of PPEGMA is small. The $(PCL_{38})_2(PDEA_{17}$-*b*-$PPEGMA_9)_2$ micelles, which proportion of PCL blocks is maximum, own a large size of the micelle core along with a high EE. However, due to the small thickness of the PDEA layer, the pH-sensitivity may not be so evident. According to the above analysis, great drug loading capacity is determined not only by the high EE of the hydrophobic block but also the protective effect of the hydrophilic shell. Although the EE of the micelles formed by $(PCL_{38})_2(PDEA_{17}$-*b*-$PPEGMA_9)_2$ with the longest hydrophobic blocks was maximum, the structure of the drug-loaded micelles shown in the simulation was of a loose shell leading to a weak protective effect on the drug-loaded micelles, thus the stability of the micelles may not in a high level. In a word, the well control on the proportion of the hydrophilic and hydrophobic components presents a profound influence on the design of micelles with expected drug loading capacity.

According to the drug distribution and drug loading capacity of the four micelles we have discussed above, longer hydrophobolic blocks do not always lead to high drug loading, it depends on the compatibility between the target drug and the hydrophobolic blocks, as well as the expected drug concentration in the micelles. Generally, longer hydrophilic blocks are in favor of the stability of the micelles but result in lower drug loading. Conversely, the pH-sensitive blocks also play an important role in the entrapment of the drugs, especially when the pH-sensitive blocks have a good compatibility of the drug.

The effect of polymeric structures on in vitro *drug release*

The well control on the proportion of the hydrophilic and hydrophobic components presents a profound influence on the design of micelles with expected *in vitro* drug release, especially the pH-sensitive blocks play a direct role. To explore the effects of different block ratios on *in vitro* drug release, DOX-loaded micelles were carried out at 37°C under different pHs (7.4, 6.5, and 5.0), as shown in Figure 10. At pH 7.4, $(PCL)_2$(PDEA-*b*-$PPEGMA)_2$ micelles were tight and the release rates were slow, only 15%–25% of DOX were released in 12 h, and approximately 28%–41% were released after 96 h. At pH 6.5, the release rates were accelerated with about 45%–57% of DOX were released after 96 h, due to the partial protonation of the tertiary amine groups of DEA contributed to the slight swelling of micelles. The release rates of DOX were greatly accelerated at pH 5.0, about 33%–38% were released in 12 h, and almost 83%–96% in 96 h, which attributed to the looser micelle structures caused by stronger protonation of tertiary amine groups in DEA moieties at lower pH conditions. And the more PDEA content, the faster cumulative release of DOX. For example, the cumulative release of DOX from $(PCL_{24})_2(PDEA_{37}$-*b*-$PPEGMA_{15})_2$ was almost 96% in 96 h, which released faster than $(PCL_{24})_2(PDEA_{16}$-*b*-$PPEGMA_{19})_2$ of 83% in 96 h. The release rates significantly accelerated as the pH decreased from 7.4 to 5.0, demonstrating that pH of the medium has a strong effect on the DOX release from the $(PCL)_2$(PDEA-*b*-$PPEGMA)_2$ micelles.

Combining the experiment results and the DPD simulations of DOX distribution and the change in the morphologies of the micelles at different pH conditions, the drug release was analyzed. The amount of the released drugs in pH 5.0 was much larger than those in pH 6.5 and pH 7.4 owing to more pH-sensitive blocks are extended in pH 5.0. The amount of DOX released from the micelles formed by the polymer with more PDEA blocks was faster than that with less PDEA components: $(PCL_{24})_2$ $(PDEA_{37}$-*b*-$PPEGMA_{15})_2 > (PCL_{38})_2$ $(PDEA_{26}$-*b*-$PPEGMA_{11})_2 > (PCL_{38})_2(PDEA_{17}$-*b*-$PPEGMA_9)_2$. It is probably because that a considerable large amount of DOX is loaded in the PDEA mesosphere (according to the discussion of the DOX distribution), and when PDEA are protonated, the stretch of the pH-sensitive chains promotes the release of DOX. Notably although the PDEA chains are short in $(PCL_{24})_2(PDEA_{16}$-*b*-$PPEGMA_{19})_2$, the drug release rate is higher than those of $(PCL_{38})_2(PDEA_{26}$-*b*-$PPEGMA_{11})_2$ and $(PCL_{38})_2(PDEA_{17}$-*b*-$PPEGMA_9)_2$. Because the length of hydrophobic components in $(PCL_{24})_2(PDEA_{16}$-*b*-$PPEGMA_{19})_2$ is small, the entrapment of DOX is not tight and a large amount of the DOX molecules distributed on the interface between the PPEGMA shell and the PDEA layer, hence these drug molecules can release easily. To sum up, the pH-sensitive blocks play a direct role in controlling the release of the drug, thus the ratio should be designed according to the drug release rate we expected. Additionally, the drug distribution in the micelles can also affect the drug release, which can be monitored by the ratios of different blocks.

Herein, the pH-induced drug release mechanism is proposed as a hypothesis based on visual inspection from the simulations. As the pH decreases, the amine groups are protonated, resulting in a rapid increase on the hydrophilicity of the PDEA chains, and subsequently the protonated PDEA chains transform to an extended shape from a collapsed shape, directly contacting to the aqueous solvent, which are regarded as the channels for the diffusion of DOX molecules, especially those distribute in PDEA intermediate layer may rapidly diffuse into water through the channels. Moreover, the protonated PDEA chains extend to the aqueous solution contacting to the water molecules, causing that the micelles tend to absorb a significant number of water molecules through the water molecule passages, which may generate a considerable pressure in the intermediate layer of micelles. This portion of PDEAH blocks may become the driving force for more water molecules to flow into the micelles and promote the swelling of the micelles. Conversely, the release of the DOX loaded in the inner of the core may be primarily controlled by diffusion, which is beneficial to the sustained release of the drugs. By contrast, the release of DOX from micelles which are unprotonated or in a very low degree of protonation requires to pass through an integrate shell and is primarily under the control of diffusion, so the release rate in this case is very slow.

Conclusions

In summary, combined with experiments, DPD simulations are successfully applied on the investigation of the drug-loaded and pH-release property of the $A_2(BC)_2$ miktoarm star polymers in neutral and acidic conditions, particularly the effects of the block ratios of the polymers on the property of the micelles were mainly discussed. The micelles containing

more PDEA contents resulted in a more prominent increase in D_hs and transmittance. The EE of DOX was higher as the hydrophobic chains get longer and the micelles with higher PDEA proportion presented a faster drug release rate. The drug release process and mechanism of the micelles were predicted via a swelling-demicellization-releasing mechanism. This multiscale study provides macroscopic and mesoscopic insight into the exploration of smart the drug delivery system, which might be useful for the optimization of the polymer structures. Also, the study demonstrated that the micelles formed by the pH-sensitive $A_2(BC)_2$ miktoarm star polymers might be a promising carrier for hydrophobic anticancer drugs, achieving controlled and sustained drug release.

Acknowledgments

This work was financially supported by National Natural Science Foundation of China (No. 21176090), Team Project of Natural Science Foundation of Guangdong Province, China (No. S2011030001366), Specialized Research Fund for the Doctoral Program of Higher Education of China (No.20130172110009), Science and Technology Foundation of Guangdong Province, China (No. 2012B050600010), and Fundamental Research Funds for the Central Universities, China (No. 2013ZP0010, 2014ZP0020).

Literature Cited

1. Langer R, Peppas NA. Advances in biomaterials, drug delivery, and bionanotechnology. *AIChE J*. 2003;49:2990–3006.
2. Wuang SC, Neoh KG, Kang ET, Leckband DE, Pack DW. Acid-sensitive magnetic nanoparticles as potential drug depots. *AIChE J*. 2011;57:1638–1645.
3. Zhuang J, Gordon MR, Ventura J, Li L, Thayumanavan S. Multi-stimuli responsive macromolecules and their assemblies. *Chem Soc Rev*. 2013;42:7421–7435.
4. Yang YQ, Lin WJ, Zhao B, Wen XF, Guo XD, Zhang LJ. Synthesis and physicochemical characterization of amphiphilic triblock copolymer brush containing pH-sensitive linkage for oral drug delivery. *Langmuir*. 2012;28:8251–8259.
5. Guo XD, Zhang LJ, Wu ZM, Qian Y. Dissipative particle dynamics studies on microstructure of pH-sensitive micelles for sustained drug delivery. *Macromolecules*. 2010;43:7839–7844.
6. Yu H, Zou Y, Wang Y, Huang X, Huang G, Sumer BD, Boothman DA, Gao J. Overcoming endosomal barrier by amphotericin B-loaded dual pH-responsive PDMA-b-PDPA micelleplexes for siRNA delivery. *ACS Nano*. 2011;5:9246–9255.
7. Shen YQ, Zhan YH, Tang JB, Xu PS, Johnson PA, Radosz M, Van Kirk EA, Murdoch WJ. Multifunctioning pH-responsive nanoparticles from hierarchical self-assembly of polymer brush for cancer drug delivery. *AIChE J*. 2008;54:2979–2989.
8. Yang YQ, Zhao B, Li ZD, Lin WJ, Zhang CY, Guo XD, Wang JF, Zhang LJ. pH-sensitive micelles self-assembled from multi-arm star triblock co-polymers poly(ε-caprolactone)-b-poly(2-(diethylamino)ethyl methacrylate)-b-poly(poly (ethylene glycol) methyl ether methacrylate) for controlled anticancer drug delivery. *Acta Biomater*. 2013;9:7679–7690.
9. Khanna K, Varshney S, Kakkar A. Miktoarm star polymers: advances in synthesis, self-assembly, and applications. *Polym Chem*. 2010;1:1171–1185.
10. Wang Y, Grayson SM. Approaches for the preparation of non-linear amphiphilic polymers and their applications to drug delivery. *Adv Drug Del Rev*. 2012;64:852–865.
11. Rosselgong J, Williams EGL, Le TP, Grusche F, Hinton TM, Tizard M, Gunatillake P, Thang SH. Core degradable star RAFT polymers: synthesis, polymerization, and degradation studies. *Macromolecules*. 2013;46:9181–9188.
12. Wang D, Chen H, Su Y, Qiu F, Zhu L, Huan X, Zhu B, Yan D, Guo F, Zhu X. Supramolecular amphiphilic multiarm hyperbranched copolymer: synthesis, self-assembly and drug delivery applications. *Polym Chem*. 2013;4:85–94.
13. Cho HY, Averick SE, Paredes E, Wegner K, Averick A, Jurga S, Das SR, Matyjaszewski K. Star polymers with a cationic core prepared by ATRP for cellular nucleic acids delivery. *Biomacromolecules*. 2013;14:1262–1267.
14. Gou PF, Zhu WP, Shen ZQ. Calixarene-centered amphiphilic A2B2 miktoarm star copolymers based on poly(ε-caprolactone) and poly (ethylene glycol): synthesis and self-assembly behaviors in water. *J Polym Sci Part A: Polym Chem*. 2010;48:5643–5651.
15. Zhang W, Zhang W, Cheng Z, Zhou N, Zhu J, Zhang Z, Chen G, Zhu X. Synthesis and aggregation behaviors of nonlinear multiresponsive, multihydrophilic block copolymers. *Macromolecules*. 2011;44:3366–3373.
16. Groot RD, Warren PB. Dissipative particle dynamics: bridging the gap between atomistic and mesoscopic simulation. *J Chem Phys*. 1997;107:4423–4435.
17. Yan LT, Zhang X. Dissipative particle dynamics simulations of complexes comprised of cylindrical polyelectrolyte brushes and oppositely charged linear polyelectrolytes. *Langmuir*. 2009;25:3808–3813.
18. Wang H, Liu YT, Qian HJ, Lu ZY. Dissipative particle dynamics simulation study on complex structure transitions of vesicles formed by comb-like block copolymers. *Polymer*. 2011;52:2094–2101.
19. Gavrilov AA, Kudryavtsev YV, Khalatur PG, Chertovich AV. Microphase separation in regular and random copolymer melts by DPD simulations. *Chem Phys Lett*. 2011;503:277–282.
20. Grafmüller A, Shillcock J, Lipowsky R. The fusion of membranes and vesicles: pathway and energy barriers from dissipative particle dynamics. *Biophys J*. 2009;96:2658–2675.
21. Xiao M, Xia G, Wang R, Xie D. Controlling the self-assembly pathways of amphiphilic block copolymers into vesicles. *Soft Matter*. 2012;8:7865–7874.
22. Smondyrev AM, Berkowitz ML. Molecular dynamics simulation of fluorination effects on a phospholipid bilayer. *J Chem Phys*. 1999;111:9864–9870.
23. Guo XD, Zhang LJ, Chen Y, Qian Y. Core/shell pH-sensitive micelles self-assembled from cholesterol conjugated oligopeptides for anticancer drug delivery. *AIChE J*. 2010;56:1922–1931.
24. Rodriguez-Hidalgo MDR, Soto-Figueroa C, Vicente L. Mesoscopic simulation of the drug release mechanism on the polymeric vehicle P(ST-DVB) in an acid environment. *Soft Matter*. 2011;7:8224–8230.
25. Lin SL, Xu MY, Yang ZR. Dissipative particle dynamics study on the mesostructures of n-octadecane/water emulsion with alternating styrene-maleic acid copolymers as emulsifier. *Soft Matter*. 2012;8:375–384.
26. Nie SY, Sun Y, Lin WJ, Wu WS, Guo XD, Qian Y, Zhang LJ. Dissipative particle dynamics studies of doxorubicin loaded micelles assembled from four-arm star triblock polymers 4AS-PCL-b-PDEAEMA-b-PPEGMA and their pH-release mechanism. *J Phys Chem B*. 2013;117:13688–13697.
27. Pasquale AJ, Long TE. Real-time monitoring of the stable free radical polymerization of styrene via in-situ mid-infrared spectroscopy. *Macromolecules*. 1999;32:7954–7957.
28. Pasquale AJ, Long TE. Synthesis of star-shaped polystyrenes via nitroxide-mediated stable free-radical polymerization. *J Polym Sci Part A: Polym Chem*. 2001;39:216–223.
29. Zhong C, Liu D. Understanding multicompartment micelles using dissipative particle dynamics simulation. *Macromol Theory Simul*. 2007;16:141–157.
30. Sheng YJ, Nung CH, Tsao HK. Morphologies of star-block copolymers in dilute solutions. *J Phys Chem B*. 2006;110:21643–21650.
31. Soto-Figueroa C, Vicente L, Martínez-Magadán JM, Rodríguez-Hidalgo MDR. Self-organization process of ordered structures in linear and star poly(styrene)-poly(isoprene) block copolymers: Gaussian models and mesoscopic parameters of polymeric systems. *J Phys Chem B*. 2007;111:11756–11764.
32. Groot RD, Madden TJ. Dynamic simulation of diblock copolymer microphase separation. *J Chem Phys*. 1998;108:8713–8724.
33. Groot RD, Madden TJ, Tildesley DJ. On the role of hydrodynamic interactions in block copolymer microphase separation. *J Chem Phys*. 1999;110:9739–9749.
34. Xin J, Liu D, Zhong C. Multicompartment micelles from star and linear triblock copolymer blends. *J Phys Chem B*. 2007;111:13675–13682.
35. Li Y, Guo Y, Bao M, Gao X. Investigation of interfacial and structural properties of CTAB at the oil/water interface using dissipative

particle dynamics simulations. *J Colloid Interface Sci.* 2011;361: 573–580.
36. Moeinzadeh S, Jabbari E. Mesoscale simulation of the effect of a lactide segment on the nanostructure of star poly(ethylene glycol-co-lactide)-acrylate macromonomers in aqueous solution. *J Phys Chem B*. 2012;116:1536–1543.
37. Li J, Chen Y, Wang Z, Ding M, Tan H, Fu Q, Jiang X. Synthesis and self-assembly of an amino-functionalized hybrid hydrocarbon/fluorocarbon double-chain phospholipid. *Langmuir*. 2011;27:10859–10866.
38. Luo Z, Jiang J. pH-sensitive drug loading/releasing in amphiphilic copolymer PAE-PEG: integrating molecular dynamics and dissipative particle dynamics simulations. *J Controlled Release*. 2012;162: 185–193.
39. Yan J, Ye Z, Chen M, Liu Z, Xiao Y, Zhang Y, Zhou Y, Tan W, Lang M. Fine tuning micellar core-forming block of poly(ethylene glycol)-block-poly(ε-caprolactone) amphiphilic copolymers based on chemical modification for the solubilization and delivery of doxorubicin. *Biomacromolecules*. 2011;12:2562–2572.
40. Chen H, Ruckenstein E. Formation and degradation of multicomponent multicore micelles: insights from dissipative particle dynamics simulations. *Langmuir*. 2013;29:5428–5434.
41. Wang WJ, Anderson NA, Travesset A, Vaknin D. Regulation of the electric charge in phosphatidic acid domains. *J Phys Chem B*. 2012; 116:7213–7220.
42. Zhang W, Zhang W, Zhou N, Zhu J, Cheng Z, Zhu X. Synthesis of miktoarm star amphiphilic block copolymers via combination of NMRP and ATRP and investigation on self-assembly behaviors. *J Polym Sci Part A: Polym Chem*. 2009;47:6304–6315.
43. Xu J, Ge Z, Zhu Z, Luo S, Liu H, Liu S. Synthesis and micellization properties of double hydrophilic A2BA2 and A4BA4 non-linear block copolymers. *Macromolecules*. 2006;39:8178–8185.
44. Zhang L, Guo R, Yang M, Jiang X, Liu B. Thermo and pH dual-responsive nanoparticles for anti-cancer drug delivery. *Adv Mater*. 2007;19:2988–2992.
45. Loh XJ, Ong SJ, Tung YT, Choo HT. Dual responsive micelles based on poly[(R)−3-hydroxybutyrate] and poly(2-(di-methylamino)ethyl methacrylate) for effective doxorubicin delivery. *Polym Chem*. 2013;4:2564–2574.
46. Yang YQ, Zheng LS, Guo XD, Qian Y, Zhang LJ. pH-sensitive micelles self-assembled from amphiphilic copolymer brush for delivery of poorly water-soluble drugs. *Biomacromolecules*. 2010;12: 116–122.
47. Lele BS, Leroux JC. Synthesis and micellar characterization of novel amphiphilic A-B-A triblock copolymers of N-(2-hydroxypropyl)-methacrylamide or N-vinyl-2-pyrrolidone with poly(ε-caprolactone). *Macromolecules*. 2002;35:6714–6723.

Manuscript received Jan. 14, 2014, and revision received June 18, 2014.